

# State-Space Constitutive Model for Magnetization and Magnetostriction of Galfenol Alloys

Phillip G. Evans and Marcelo J. Dapino

Department of Mechanical Engineering, The Ohio State University, Columbus, OH 43210 USA

**We present a thermodynamic model that quantifies the magnetization and magnetostriction of annealed or unannealed Galfenol alloys subjected to magnetic fields and mechanical stresses. The model requires a small number of parameters directly related to physical properties of the data, thus providing a useful tool for material characterization and design. Furthermore, the model is formulated in state-space form, which simplifies computations for design and control of Galfenol devices.**

**Index Terms**—Constitutive model, Galfenol, state-space formulation, thermal relaxation.

## I. INTRODUCTION

**G**ALFENOL ( $\text{Fe}_{1-x}\text{Ga}_x$ ) is an emerging new magnetostrictive material that possesses fundamental advantages. Unlike most active materials, Galfenol is malleable and machinable, and can be safely operated in tension, compression, bending, and under shock loads. Due to Galfenol's unique combination of metallurgical and mechanical properties, it has the potential to enable smart load-bearing devices and structures in innovative 3-D geometries manufactured by welding, extrusion, rolling, deposition, or machining. Further, the control of anisotropies through manufacturing and post-processing methods made possible with Galfenol could lead to innovative devices with fully coupled 3-D functionality. Examples include nanowires for acoustic sensors that mimic the hairlike cilia of the inner ear [1], sonar transducers with load-bearing properties and adaptive 3-D projection patterns, and shock-tolerant adaptive structures.

Previous models for Galfenol [2], [3] have followed Armstrong's approach [4] of using a single energy-weighted average of the Gibbs free energy for the entire material to calculate the distribution of moments. The weighting function tends to smooth the sharp magnetization and magnetostriction transitions obtained by direct minimization of the Gibbs free energy, thus providing a more accurate description of physical measurements. However, the weighting function depends on a nonphysical parameter. Because the moment volume fractions are not tracked, this model cannot characterize the hysteresis due to anisotropy or rate dependent thermal effects, which occurs because of the history dependence of the moment volume fractions in each Gibbs energy well.

In this paper, we present a macroscopic constitutive model that accurately quantifies hysteresis, stress and annealing-induced anisotropies, and thermal relaxation effects present in the magnetization and magnetostriction of general magnetostrictive materials, with especial consideration to Galfenol's specific properties. Our approach consists of finding a local magnetization kernel through minimization of the Gibbs free energy of a single magnetic moment and then applying Boltzmann statistics to calculate the evolution of moment volume fractions in the bulk material. We formulate the model in state-space form, which greatly simplifies model implementation for large-signal

(i.e., nonlinear) device design and control. The model requires a small number of parameters that can be correlated with physical properties of the data.

In our approach, thermal energy creates a Boltzmann distribution of moments in each of the Gibbs energy wells and causes moments to jump between wells. The bulk magnetization and magnetostriction are calculated by tracking the volume fraction of moments in each well and summing their expected contribution to the bulk magnetization or magnetostriction. The result is a linear time-variant equation that is expressed in state-space form. The modeling of a nonlinear time-invariant system as a linear time-variant system is advantageous because the stability properties of such systems are well understood (see, for example, [5]).

## II. MODEL DEVELOPMENT

### A. Energy Formulations

The Helmholtz free energy  $\psi$  is given by the Legendre transformation of the internal energy  $U$ ,  $\psi = U - \theta\eta$ , where  $\theta$  is temperature and  $\eta$  is entropy. The internal energy is comprised of magnetocrystalline anisotropy energy  $U_a$  and stress-induced anisotropy energy  $U_T$ .

The magnetocrystalline anisotropy energy depends on the orientation  $\hat{\mathbf{m}} = [\hat{m}_x, \hat{m}_y, \hat{m}_z]$  of the magnetization. Stress-annealed Galfenol has tetragonal crystal symmetry [2] for which  $U_a$  has been given in [6]

$$U_a(\hat{\mathbf{m}}) = K_2 \left( \hat{m}_z^2 - \frac{1}{3} \right) + K_4 \left( \hat{m}_x^4 + \hat{m}_y^4 + \hat{m}_z^4 - \frac{3}{5} \right) + K_{4'} \left( \hat{m}_z^4 - \frac{6}{7} \hat{m}_z^2 + \frac{3}{35} \right). \quad (1)$$

The  $x$ ,  $y$ , and  $z$  spatial directions are assumed to be aligned with the [100], [010], and [001] crystal directions. The constant  $K_4$  is the fourth-order cubic anisotropy constant and the constants  $K_2$  and  $K_{4'}$  are the second-order and fourth-order uniaxial anisotropy constants that favor or penalize the  $z$  direction depending on their sign. Recognizing that  $\hat{m}_x^2 + \hat{m}_y^2 + \hat{m}_z^2 = 1$ ,  $K_4$  can be shown to be related to  $K_1$  in the traditional cubic formulation (used, for example, in [4])

$$E = K_0 + K_1 (\hat{m}_x^2 \hat{m}_y^2 + \hat{m}_y^2 \hat{m}_z^2 + \hat{m}_z^2 \hat{m}_x^2) + \dots \quad (2)$$

by  $2K_4 = -K_1$ . Rafique *et al.* [7] measured  $K_1$  for single-crystal Galfenol alloys with 5–20 at.% Ga. We use a  $K_4$  value

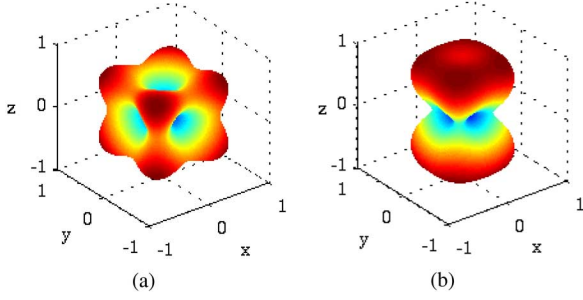


Fig. 1. Comparison of (a) unannealed and (b) annealed Helmholtz free energies with no applied stress. The energy has been normalized and is proportional to the distance from the origin and the color.

that is about 40% lower than the corresponding  $K_4$  value obtained from the  $K_1$  coefficients presented in [7]. The difference is due to our samples being highly textured polycrystals rather than single crystals.

The stress anisotropy, which is induced by the magnetoelastic coupling energy, depends on the stress tensor  $T_{ij}$  in a manner dictated by the crystal symmetry. The derivation of the stress anisotropy from the magnetoelastic coupling energy for materials exhibiting cubic symmetry in the magnetostriction has been presented by Kittel [8]. The stress contribution to the anisotropy is

$$U_T(\hat{\mathbf{m}}, T_{ij}) = -(3/2)\lambda_{001}(\hat{m}_x^2 T_{xx} + \hat{m}_y^2 T_{yy} + \hat{m}_z^2 T_{zz}) - 3\lambda_{111}T(\hat{m}_x \hat{m}_y T_{xy} + \hat{m}_y \hat{m}_z T_{yz} + \hat{m}_z \hat{m}_x T_{zx}) \quad (3)$$

where  $\lambda_{001}$  and  $\lambda_{111}$  are magnetostriction along the [001] and [111] directions, respectively.

By considering only isothermal processes and incorporating irreversibilities into the moment rotations (see Section II-D) rather than through a direct entropy formulation, the Helmholtz free energy reduces to the internal energy  $\psi = U_a(\hat{\mathbf{m}}) + U_T(\hat{\mathbf{m}}, T_{ij})$ .

Fig. 1 shows the effect of stress-annealing or compressive stresses along the  $z$ -axis on the Helmholtz free energy. The  $z$ -direction becomes a higher energy direction, which has two effects on the magnetization due to magnetic fields applied in this direction. First, the hysteresis and remanence magnetization decrease because there is no longer a deep energy well to trap magnetic moments. Second, higher fields are required to saturate the material. The depth of the wells on the  $z$ -axis is determined by the magnitude and sign of  $K_2$  and  $K'_4$  relative to  $K_4$ . In the case when  $K_2$  and  $K'_4$  are zero as in Fig. 1(a), relation (1) is identical to (2) up to the  $K_1$  term and the symmetry is cubic.

The Gibbs free energy of a single magnetic moment is obtained through the Legendre transformation  $G = \psi - \mu_0 M_s \hat{\mathbf{m}} \cdot \mathbf{H}$ , where  $M_s$  is the saturation magnetization and  $\mathbf{H}$  is an applied magnetic field. In the common case in which the applied magnetic field and stress are oriented along the  $z$ -axis, the Gibbs free energy has the form

$$G = K_4(\hat{m}_x^4 + \hat{m}_y^4 + \hat{m}_z^4) + K'_4 \hat{m}_z^4 + \left(K_2 - \frac{6}{7}K'_4 - \frac{3}{2}\lambda_{001}T\right)\hat{m}_z^2 - \mu_0 M_s H \hat{m}_z \quad (4)$$

where  $H$  is the magnetic field and  $T$  is the stress along the  $z$ -axis. Constant terms have been omitted because it is the change in the Gibbs energy that determines the moment orientation. The Gibbs energy (4) is expressed more efficiently in spherical coordinates with the orientation of the magnetization vector defined by the angle  $\phi$  it makes with the  $z$ -axis and the angle  $\alpha$  that its projection in the  $x$ - $y$  plane makes with the  $x$ -axis

$$G = K_4(\sin^4 \phi (\sin^4 \alpha + \cos^4 \alpha) + \cos^4 \phi) + K'_4 \cos^4 \phi + \left(K_2 - \frac{6}{7}K'_4 - \frac{3}{2}\lambda_{001}T\right)\cos^2 \phi - \mu_0 M_s H \cos \phi. \quad (5)$$

When thermal energy and material defects are negligible, all of the magnetic moments will be oriented in the locally minimum directions in each of the energy wells. The bulk magnetization is the vector sum of the magnetization due to each magnetic moment. Therefore, to determine the bulk magnetization one requires an equation for the trajectory of the energy wells produced by applied magnetic fields and the volume fraction of moments in each well. The symmetry in the 3-D Gibbs energy implies that the moments in each of the four energy wells in the basal plane follow the same  $\phi$  path when an applied magnetic field in the  $z$ -direction induces rotation of moments into the field direction. It is sufficient then to model the trajectory of just one of these wells because the contribution to the magnetization in the  $z$ -direction of moments lying in any of the four wells will be the same [Fig. 2(a), (c), (e)]. Choosing the energy well in the  $x$ -direction ( $\alpha = 0$ ) to be tracked and using only cos functions, (5) becomes

$$G = (2K_4 + K'_4)\cos^4 \phi + \left(K_2 - \frac{6}{7}K'_4 - 2K_4 - \frac{3}{2}\lambda_{001}T\right)\cos^2 \phi - \mu_0 M_s H \cos \phi. \quad (6)$$

This reduced-dimension energy potential is shown in Fig. 2(b), (d), (f) beside the 3-D energy potential (4). Minimization of (6) yields the  $\phi$  orientation of the energy wells. Since  $K_4$  and  $K'_4$  always contribute together and in nearly the same proportion, we neglect  $K'_4$  as was done in the anhysteretic model of Restorff *et al.* [2].

Gibbs energy (6) was derived for single crystals under uniaxial compression. However, it is also appropriate for highly textured polycrystals having negligible grain misalignment. Consider for example a grain with a five degree misalignment of the [001] direction with the axis of a rod subjected to a compressive stress  $T$  along the axis ( $z$ -direction). The stress state in the rod reference frame would be  $[T_x, T_y, T_z, T_{xy}, T_{yz}, T_{zx}] = T[0, 0, 1, 0, 0, 0]$  while the stress state in the grain reference frame would be  $T[0.001523, 0, 0.999999, 0, 0, 0.001523]$ , which is approximately uniaxial. To accommodate lower grade polycrystals having appreciable grain misalignment, the tensorial stress-induced anisotropy energy (3) would need to be used along with a homogenization technique like that of Appino, Valsania, and Basso [9] to characterize the distribution of grain orientations.

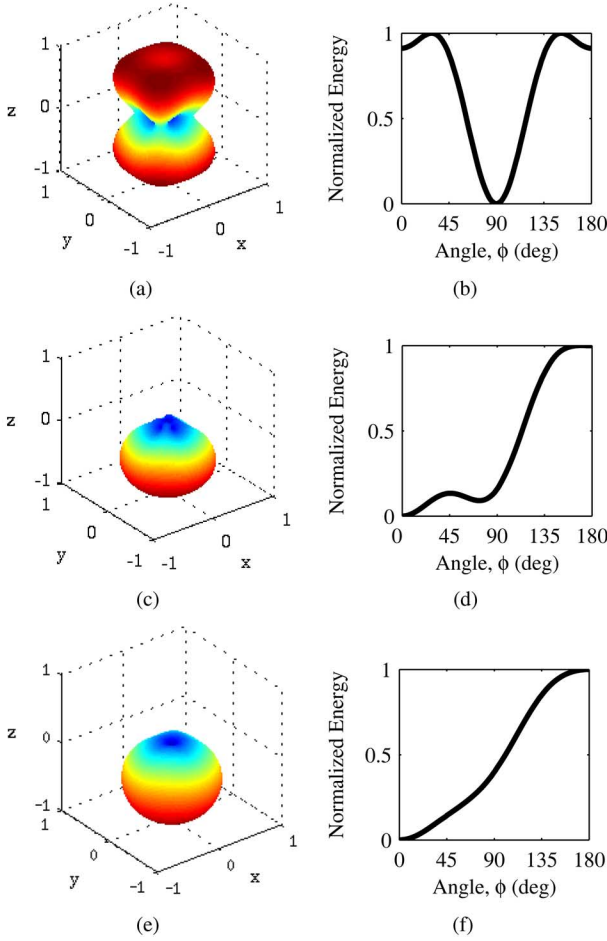


Fig. 2. Left column: 3-D Gibbs free energy given by (4). Right column: Reduced 2-D Gibbs free energy given by (6). The rows represent low, medium, and high magnetic fields (top to bottom).

### B. Local Magnetization

The orientation of a single magnetic moment is determined by two conditions,  $\partial G/\partial \phi = 0$  and  $\partial^2 G/\partial \phi^2 > 0$ . Application of the first condition to (6), followed by factorization gives

$$8K_4 \cos^3 \phi + 2 \left( K_2 - 2K_4 - \frac{3}{2} \lambda_{001} T \right) \cos \phi - \mu_0 M_s H = 0, \quad (7)$$

$$\sin \phi = 0. \quad (8)$$

Relation (8) coupled with the second condition simply identifies the easy axes in the positive and negative  $z$ -directions and their intervals of existence. The positive  $z$ -direction is a minimum energy direction on the interval  $[2(2K_4 + K_2 - 3/2\lambda_{001}T)/\mu_0 M_s, +\infty)$  and the negative  $z$ -direction is a minimum energy direction on the interval  $(-\infty, -2(2K_4 + K_2 - 3/2\lambda_{001}T)/\mu_0 M_s]$ . Magnetic fields outside of the first interval will cause the easy axis in the positive  $z$ -direction to become hard and magnetic fields outside of the second interval will cause the easy axis in the negative  $z$ -direction to become hard.

Relation (7) is a cubic equation in  $\cos \phi$  that can be solved analytically with Cardano's method. The three solutions give the  $\phi$  location of the two energy maxima and the energy minimum

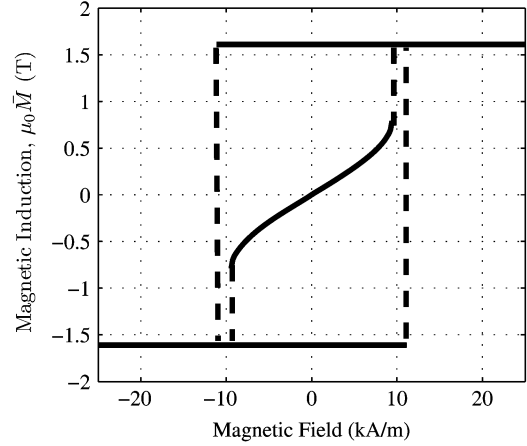


Fig. 3. Local magnetization hysteron obtained from minimization of the Gibbs free energy.

in Fig. 2(a). The discriminant in Cardano's method can be used to determine the interval of existence of the energy minimum; this yields a simpler solution than the condition on the second derivative of the Gibbs energy. Setting the discriminant equal to zero yields the interval of existence

$$|H| \leq -16 \frac{K_4}{\mu_0 M_s} \left( \frac{2K_4 - K_2 + \frac{3}{2} \lambda_{001} T}{12K_4} \right)^{3/2}. \quad (9)$$

The hysteretic, local magnetization in the  $z$ -direction (Fig. 3) is constructed from the relation  $\bar{M} = M_s \cos \phi$ , in which possible values of  $\phi$  are the solutions to (7) and (8) with their respective magnetic field intervals of existence. The result is a triple valued hysteron in which the cubic branch that passes through the origin accounts for the low hysteresis and characteristic "S" shape of the  $M-H$  major loop of bulk Galfenol. The shallow slope and finite interval of existence of the cubic branch is a manifestation of the rotation of magnetic moments away from the four energy wells in the  $xy$ -plane into the direction of the applied magnetic field and the eventual disappearance of these wells.

### C. Local Anhyseretic Magnetization

At low magnetic field levels and in cases when a compressive stress is applied or stress-annealed Galfenol is used, the energy wells that give rise to the cubic branch of the kernel are much deeper than the wells that give rise to the saturation solutions. As a result, at low magnetic fields most of the magnetic moments will reside in these energy wells and the bulk magnetization will follow the cubic branch of the kernel. The slope of the cubic branch at zero field can be obtained through a linear approximation to (7)

$$\bar{M} = \frac{(\mu_0 M_s)^2}{2(K_2 - 2K_4 - \frac{3}{2} \lambda_{001} T)} H \quad (10)$$

$$\frac{d\bar{M}}{dH}(H=0) = \frac{(\mu_0 M_s)^2}{2(K_2 - 2K_4 - \frac{3}{2} \lambda_{001} T)}. \quad (11)$$

Under the assumption that the bulk magnetization follows the cubic branch closely at low fields, (11) provides a useful measure of the anisotropy since  $d\bar{M}/dH(H=0)$ ,  $\lambda_{001}$ , and  $\mu_0 M_s$

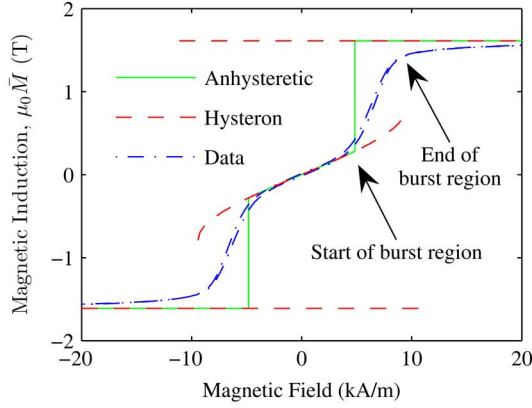


Fig. 4. Anhyseretic magnetization calculated from the measured magnetization curve of  $\text{Fe}_{81.6}\text{Ga}_{18.4}$ . The following values were observed from the data using (11) and (12):  $K_4 = -8.0 \text{ kJ/m}^3$ ,  $K_2 = -0.10 \text{ kJ/m}^3$ ,  $\mu_0 M_s = 1.61 \text{ T}$ , and  $(3/2)\lambda_{001} = 260 \mu\text{strain}$ .

are all easily measured. This assumption is accurate for sufficiently high compressive stress.

A second measure of the anisotropy is necessary since there are two anisotropy coefficients. As the applied magnetic field is increased or decreased from zero, it reaches a level where the energy well of the saturation solution in the direction of the applied field becomes deeper than the energy wells of the cubic branch. At this point, rapid jumping of magnetic moments occurs from the energy wells of the cubic branch to the energy well of the saturation solution. This situation is evident in the burst region of the magnetization curve. A close approximation of the field level that will initiate the burst region can be found analytically by equating the Gibbs energy (6) evaluated on the saturation solution with the Gibbs energy evaluated on the linear approximation of the cubic branch (10). This yields

$$H_B = \frac{2(2K_4 - K_2 + 3/2\lambda_{001}T)}{\mu_0 M_s} \cdot \left( \sqrt{\frac{K_2 - 3/2\lambda_{001}T}{2K_4 - K_2 + 3/2\lambda_{001}T}} - 1 - 1 \right). \quad (12)$$

Since the transition into the burst region of the measured magnetization curve is smooth, it is not possible to measure  $H_B$  exactly. However, a first approximation of the anisotropy constants can be obtained by assuming that  $H_B$  is the start of the linear portion of the burst region (which is observable in data, see Fig. 4) and then using relations (11) and (12). This point is more clearly identifiable when either a moderate compressive stress is applied or the material has been stress-annealed.

The anhyseretic curve is generated by forcing all of the magnetic moments to follow the cubic branch of the kernel until the saturation branches become the global minima at fields above  $H_B$  or below  $-H_B$  (Fig. 4). This anhyseretic curve does not closely follow actual magnetization curves due to the effects of thermal energy. However, relations (11) and (12) do provide an approximate measure of the anisotropy coefficients without the need of a least-squares fitting procedure to a full model. Furthermore, these relations could be used in transducer design to

select the mechanical prestress needed to achieve a prescribed magnetization, and hence magnetostriction, response.

The magnetization kernel also provides insight into the magnetization process. Since the energy wells of the cubic branch shrink continuously with increasing fields until they disappear, it is expected that by the time they disappear, nearly all of the moments have jumped to the saturation branch. Thus, the end point of the cubic branch can be interpreted as the end of the burst region. Fig. 4 shows the theoretical anhyseretic curve and kernel along with Galfenol data. The material is unannealed  $\text{Fe}_{81.6}\text{Ga}_{18.4}$  subjected to a constant compressive stress of 27.6 MPa. The anisotropy constants were approximated using (11) and (12).

#### D. Thermal Energy

As proposed by Néel [10], thermal energy causes precession of magnetic moments about local energy minima and jumping between energy wells. Following the approach of Smith *et al.* [11], we assume that the magnetic moments follow a Boltzmann distribution within each energy well and that Boltzmann statistics quantify the likelihood that moments overcome the barrier between adjacent wells. Since jumping between the four energy wells in the  $xy$ -plane and precession in the  $\theta$  coordinate have little effect on the magnetization or strain in the  $z$ -direction, we neglect these effects and continue using the reduced-dimension Gibbs energy (6).

The expected value of magnetization in the  $z$ -direction of moments residing in each of the energy wells can be calculated from the assumed Boltzmann distribution (with  $k\theta/V$  the ratio of Boltzmann constant, temperature, and effective moment volume) [11]

$$\begin{aligned} \langle \bar{M} \rangle_+ &= \frac{\int_{M_0}^1 \mu_0 M_s \bar{M}_r e^{-G(\bar{M}_r, T, H)V/k\theta} d\bar{M}_r}{\int_{M_0}^1 e^{-G(\bar{M}_r, T, H)V/k\theta} d\bar{M}_r}, \\ \langle \bar{M} \rangle_c &= \frac{\int_{-M_0}^{M_0} \mu_0 M_s \bar{M}_r e^{-G(\bar{M}_r, T, H)V/k\theta} d\bar{M}_r}{\int_{-M_0}^{M_0} e^{-G(\bar{M}_r, T, H)V/k\theta} d\bar{M}_r}, \\ \langle \bar{M} \rangle_- &= \frac{\int_{-1}^{-M_0} \mu_0 M_s \bar{M}_r e^{-G(\bar{M}_r, T, H)V/k\theta} d\bar{M}_r}{\int_{-1}^{-M_0} e^{-G(\bar{M}_r, T, H)V/k\theta} d\bar{M}_r}. \end{aligned} \quad (13)$$

Here,  $\langle \bar{M} \rangle_+$ ,  $\langle \bar{M} \rangle_c$ , and  $\langle \bar{M} \rangle_-$  are the expected values of magnetization of moments residing in the energy wells associated with the positive saturation branch, the cubic branch, and the negative saturation branch of the kernel, respectively. The integration limit  $M_0 = \cos \phi_0$  is the location of the energy hump that separates the energy wells and  $\bar{M}_r = \cos \phi$  is the relative magnetization in the  $z$ -direction (Fig. 5).

To calculate the bulk magnetization, both the volume fraction of moments residing in each energy well and the expected values of magnetization for each energy well are needed. This requires knowledge of the initial distribution and the rates at which moments jump between energy wells. When a magnetic moment is excited to the inflection point in the Helmholtz free energy, it has enough energy to jump to the adjacent energy well [12]. The probabilities  $p_{i,j}$  of a magnetic moment jumping from an initial

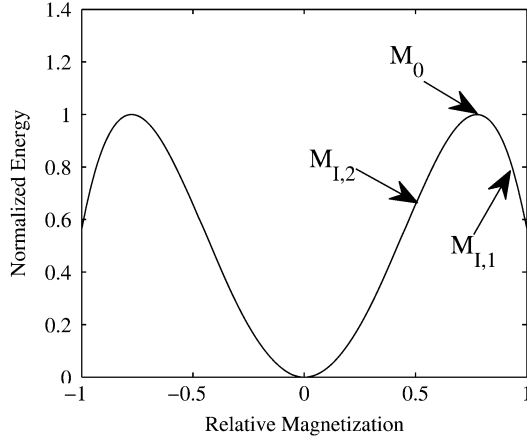


Fig. 5. Two-dimensional representation of the Helmholtz free energy.

energy well  $i$  ( $i = +, c, -$ ) to a destination well  $j$  ( $j = +, c, -$ ) are [11]

$$\begin{aligned}
 p_{+,c} &= \frac{1}{\tau} \frac{\int_{M_{I,1}-\epsilon}^{M_{I,1}} e^{-G(\bar{M}_r, T, H)V/k\theta} d\bar{M}_r}{\int_{M_{I,1}-\epsilon}^1 e^{-G(\bar{M}_r, T, H)V/k\theta} d\bar{M}_r}, \\
 p_{c,+} &= \frac{1}{\tau} \frac{\int_{M_{I,2}}^{M_{I,2}+\epsilon} e^{-G(\bar{M}_r, T, H)V/k\theta} d\bar{M}_r}{\int_0^{M_{I,2}+\epsilon} e^{-G(\bar{M}_r, T, H)V/k\theta} d\bar{M}_r}, \\
 p_{c,-} &= \frac{1}{\tau} \frac{\int_{-M_{I,2}}^{-M_{I,2}-\epsilon} e^{-G(\bar{M}_r, T, H)V/k\theta} d\bar{M}_r}{\int_{M_{I,2}}^0 e^{-G(\bar{M}_r, T, H)V/k\theta} d\bar{M}_r}, \\
 p_{-,c} &= \frac{1}{\tau} \frac{\int_{-M_{I,1}}^{-M_{I,1}+\epsilon} e^{-G(\bar{M}_r, T, H)V/k\theta} d\bar{M}_r}{\int_{-1}^{-M_{I,1}+\epsilon} e^{-G(\bar{M}_r, T, H)V/k\theta} d\bar{M}_r}. \quad (14)
 \end{aligned}$$

The proportionality constant  $1/\tau$  is the frequency at which moments attempt to jump, with  $\tau$  the thermal relaxation time constant. The integral bounds  $M_{I,1}$  and  $M_{I,2}$  are the inflection points on either side of the energy humps in the Helmholtz free energy (Fig. 5) that may be found as the positive roots of the second derivative of the Gibbs energy (6) under zero field. The parameter  $\epsilon$  is the width of a small interval of relative magnetization that includes the inflection point in the Helmholtz energy. Because  $\epsilon$  has to be small compared to the width of the energy wells, the integrals in the numerators of (14) can be evaluated using right endpoint numerical integration

$$\int_{M_{I,1}-\epsilon}^{M_{I,1}} e^{-G(\bar{M}_r, T, H)V/k\theta} d\bar{M}_r \approx \epsilon e^{-G(M_{I,1}, T, H)V/k\theta}. \quad (15)$$

This approximation allows us to define a time constant ratio,  $\bar{\tau}_i = \tau/\epsilon_i$ ,  $i = 1, 2$ , in which index  $i$  is 1 for the positive and negative energy wells and 2 for the cubic energy well. The unit of measure for  $\bar{\tau}_i$  is seconds because  $\epsilon_i$  is unitless. The time constant ratio is treated as a parameter to be identified from experimental data. Assuming a typical time constant  $\tau = 1 \times 10^{-9}$  s, the integration intervals are calculated to vary between  $5.3 \times 10^{-9}$  and  $2.5 \times 10^{-10}$  depending on stress, annealing, and which energy well is considered (Tables II and III). These values are sufficiently small relative to the width of the positive,

TABLE I  
MODEL PARAMETERS

$K_4$	Anisotropy coefficient
$K_2$	Anisotropy coefficient
$3/2\lambda_{001}$	Saturation magnetostriction
$\mu_0 M_s$	Saturation magnetic flux density (intrinsic)
$k\theta/V$	Boltzmann constant, temperature, effective volume
$\bar{\tau}_1$	Time constant ratio for the positive and negative wells
$\bar{\tau}_2$	Time constant ratio for the cubic well

TABLE II  
PARAMETER OPTIMIZATION FOR UNANNEALED Fe<sub>81.6</sub>Ga<sub>18.4</sub>  
AT FOUR STRESS LEVELS

Case	1	2	3	4
T MPa	-1.38	-13.9	-27.6	-41.4
$K_4$ kJ/m <sup>3</sup>	-6.44	-6.64	-6.89	-9.37
$K_2$ kJ/m <sup>3</sup>	-1.23	-0.455	0.182	-0.173
$k\theta/V$ kJ/m <sup>3</sup>	0.552	0.519	0.404	0.458
$\bar{\tau}_1$ sec	0.918	1.69	1.90	1.53
$\bar{\tau}_2$ sec	0.190	0.349	0.392	0.317
Maximum % error	1.2	1.2	0.70	0.96

TABLE III  
PARAMETER OPTIMIZATION FOR ANNEALED Fe<sub>81.6</sub>Ga<sub>18.4</sub>  
AT FOUR STRESS LEVELS

Case	1	2	3	4
T MPa	-1.38	-13.9	-27.6	-41.4
$K_4$ kJ/m <sup>3</sup>	-8.29	-10.0	-1.26	-9.07
$K_2$ kJ/m <sup>3</sup>	15.6	15.6	15.8	13.8
$k\theta/V$ kJ/m <sup>3</sup>	0.878	0.994	1.09	0.956
$\bar{\tau}_1$ sec	4.07	4.35	3.95	NA
$\bar{\tau}_2$ sec	0.841	0.898	0.815	NA
Maximum % error	0.64	0.85	0.85	1.7

negative, and cubic energy wells, which have the relative magnetization values of 0.3172 ( $1 - M_0$ ), 0.3172( $-M_0 + 1$ ), and 1.3656 ( $2 \cdot M_0$ ), respectively.

With the jumping probabilities (14), the evolution of the moment volume fraction in each energy well,  $X_i$  ( $i = +, c, -$ ), can be expressed as

$$\begin{aligned}
 \dot{X}_+ &= -p_{+,c}X_+ + p_{c,+}X_c, \\
 \dot{X}_c &= p_{+,c}X_+ - (p_{c,+} + p_{c,-})X_c + p_{-,c}X_-, \\
 \dot{X}_- &= p_{c,-}X_c - p_{-,c}X_-. \quad (16)
 \end{aligned}$$

Implicit in model (13)–(16) is the assumption that the rate at which thermal equilibrium is achieved within each energy well is much faster than the rate at which moments jump between wells. This justifies the local use of the Boltzmann probability in (13)–(14) that is derived assuming thermal equilibrium (see [13, pp. 104–108] for details). Analogous kinetic models have

been used to characterize the quasi-static behavior of piezoelectric and shape-memory materials [14], [15]. The bulk magnetization can now be obtained by integrating (16) and summing the products of the volume fractions and their respective expected value of magnetization

$$M = \langle \hat{M} \rangle_+ X_+ + \langle \hat{M} \rangle_c X_c + \langle \hat{M} \rangle_- X_- . \quad (17)$$

Equations (16) and (17) can be assembled in state-space form to yield a linear, time-variant system of the form

$$\begin{aligned} \dot{\mathbf{X}} &= \mathbf{A}(t)\mathbf{X}, \\ M &= \mathbf{C}_M(t)\mathbf{X} \end{aligned} \quad (18)$$

where  $\mathbf{X}$  is the vector of volume fractions,  $\mathbf{A}(t)$  is the matrix of field dependent jumping probabilities, and  $\mathbf{C}_M(t)$  is the vector of field dependent expected values of magnetization. System (18) depends only on the input magnetic field, applied stress, and the six material constants in Table I.

The thermal quantity  $k\theta/V$  is interpreted as the thermal energy per volume, where the volume is that of a single rotational element. This volume changes with field and varies throughout the material because three distinct rotations take place: coherent rotation of moments (domain rotation), incoherent rotation of moments within domains (moment precession), and rotation of single moments at domain walls (domain wall motion). Domain rotation occurs in the high permeability burst region, moment precession at all field levels, and domain wall motion mainly in the low field region [16]. To preserve the low order of the model we do not attempt to characterize the domain configuration and hence use a constant volume that is determined through a least squares fit to the data ( $V = 8.09 \times 10^{-24} \text{ m}^3$ , or the volume of a sphere with radius 12 nm).

While the hysteron described by relations (7) and (8) and shown in Fig. 3 does not appear explicitly in the model (18), the model converges to the hysteron as the thermal energy decreases, i.e., as the quantity  $k\theta/V$  decreases. This was shown in [11] for a double well potential and is illustrated in Fig. 6 for the triple well potential (6).

### E. Magnetostriction Model

Kellogg *et al.* [17] experimentally quantified the nonlinear relationship between the magnetostriction and the square of the magnetization, concluding that the magnetization process does not occur solely from  $90^\circ$  moment rotation. Since this agrees with the magnetization model developed in Section II-D, we follow the same approach for the magnetostriction model. Probabilities (14) remain unchanged. We simply need to calculate the expected value of the strain contribution of moments residing in each energy well and sum their product with the volume fractions calculated from integration of (16). With cubic crystal symmetry the relationship between the magnetization and magnetostriction under axially applied stresses

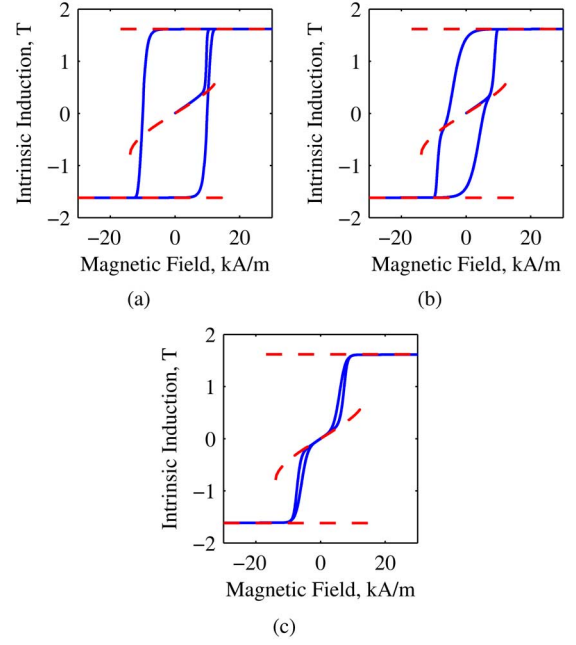


Fig. 6. Bulk magnetization model (18) calculated for the cases: (a) low thermal energy, (b) medium thermal energy, and (c) high thermal energy compared to the local hysteron described by relations (7) and (8).

and negligible thermal activation is  $\bar{S} = (3/2)\lambda_{001} \cos^2 \phi$  [8]. The effect of thermal energy is quantified as in Section II-D by classical Boltzmann statistics. The expected values of the magnetostriction thus are

$$\begin{aligned} \langle \bar{S} \rangle_+ &= \frac{\int_{M_0}^1 \frac{3}{2} \lambda_{001} \bar{M}_r^2 e^{-G(\bar{M}_r, T, H)V/k\theta} d\bar{M}_r}{\int_{M_0}^1 e^{-G(\bar{M}_r, T, H)V/k\theta} d\bar{M}_r}, \\ \langle \bar{S} \rangle_c &= \frac{\int_{-M_0}^{M_0} \frac{3}{2} \lambda_{001} \bar{M}_r^2 e^{-G(\bar{M}_r, T, H)V/k\theta} d\bar{M}_r}{\int_{-M_0}^{M_0} e^{-G(\bar{M}_r, T, H)V/k\theta} d\bar{M}_r}, \\ \langle \bar{S} \rangle_- &= \frac{\int_{-1}^{-M_0} \frac{3}{2} \lambda_{001} \bar{M}_r^2 e^{-G(\bar{M}_r, T, H)V/k\theta} d\bar{M}_r}{\int_{-1}^{-M_0} e^{-G(\bar{M}_r, T, H)V/k\theta} d\bar{M}_r}. \end{aligned} \quad (19)$$

These are assembled into the output vector  $\mathbf{C}_S(t)$  to yield a state-space magnetostriction model of the same form as (18)

$$\begin{aligned} \dot{\mathbf{X}} &= \mathbf{A}(t)\mathbf{X}, \\ S &= \mathbf{C}_S(t)\mathbf{X}. \end{aligned} \quad (20)$$

This system also depends only on the input field, applied bias stress, and the material parameters in Table I.

### F. Bulk Anhyseretic Model

The anhyseretic magnetization and magnetostriction are given by the steady-state solution to systems (18) and (20)

$$\begin{aligned} M_{\text{an}} &= \mathbf{C}_M \mathbf{X}_{\text{ss}}, \\ S_{\text{an}} &= \mathbf{C}_S \mathbf{X}_{\text{ss}}. \end{aligned}$$

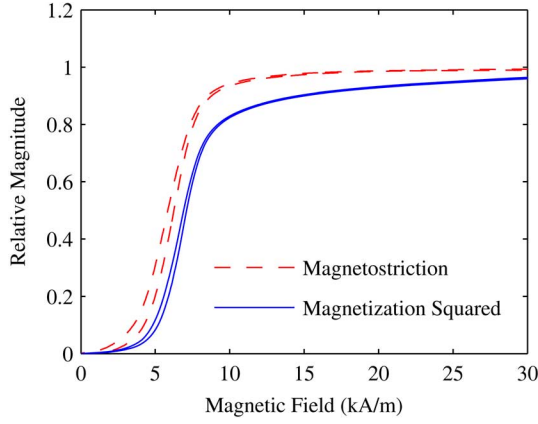


Fig. 7. High field measurement of  $\text{Fe}_{81.6}\text{Ga}_{18.4}$  with 27.6 MPa preload.

The components of the steady state vector  $\mathbf{X}_{ss}$  are calculated from  $\mathbf{A}(t)\mathbf{X} = \mathbf{0}$  and the conservation relation  $X_+ + X_c + X_- = 1$

$$\begin{aligned} X_{+,ss} &= \frac{p_{c,+}(p_{-,c} + p_{c,-}) - p_{c,+}p_{c,-}}{(p_{+,c} + p_{c,+})(p_{-,c} + p_{c,-}) - p_{c,+}p_{c,-}}, \\ X_{-,ss} &= \frac{p_{c,-}(p_{+,c} + p_{c,+}) - p_{c,-}p_{c,+}}{(p_{+,c} + p_{c,+})(p_{-,c} + p_{c,-}) - p_{c,+}p_{c,-}}, \\ X_{c,ss} &= 1 - X_{+,ss} - X_{-,ss}. \end{aligned}$$

The steady-state anhysteretic model may be used to quantify the magnetostriction and magnetization of materials with small  $\tau$  and in cases when the input magnetic field varies slowly. Fig. 8 illustrates the convergence of the hysteretic model to the anhysteretic model as  $\tau$  is decreased. As  $\tau$  is decreased, the delay decreases and so does the hysteresis.

### G. High Stress or Stress Annealing

When the prestress or the uniaxial anisotropy constant  $K_2$  exceed a critical value, the Helmholtz energy becomes a single-well potential. In this case, all of the moments reside in the same well and there is no hysteresis due to anisotropy. This situation occurs when the unstable equilibrium  $M_0$  of the Helmholtz free energy (see Fig. 5) is greater than unity. The level of stress or uniaxial anisotropy that produces  $M_0 = 1$  can be found by expressing  $M_0$  explicitly from  $d\psi/d\phi = 0$ , setting it equal to unity, and solving for  $T$  or  $K_2$ . This gives

$$\begin{aligned} T &= \frac{2}{3\lambda_{001}} 2K_4 + K_2, \\ K_2 &= \frac{3}{2}\lambda_{001}T - 2K_4. \end{aligned}$$

With a single-well Helmholtz potential there are no moment jumping effects due to thermal energy. However, thermal energy does create a Boltzmann distribution of moments within the well. Thus, for a single-well potential, the magnetization and magnetostriction can be modeled as

$$M = \frac{\int_{-1}^1 \mu_0 M_s \bar{M}_r e^{-G(\bar{M}_r, T, H)V/k\theta} d\bar{M}_r}{\int_{-1}^1 e^{-G(\bar{M}_r, T, H)V/k\theta} d\bar{M}_r} \quad (21)$$

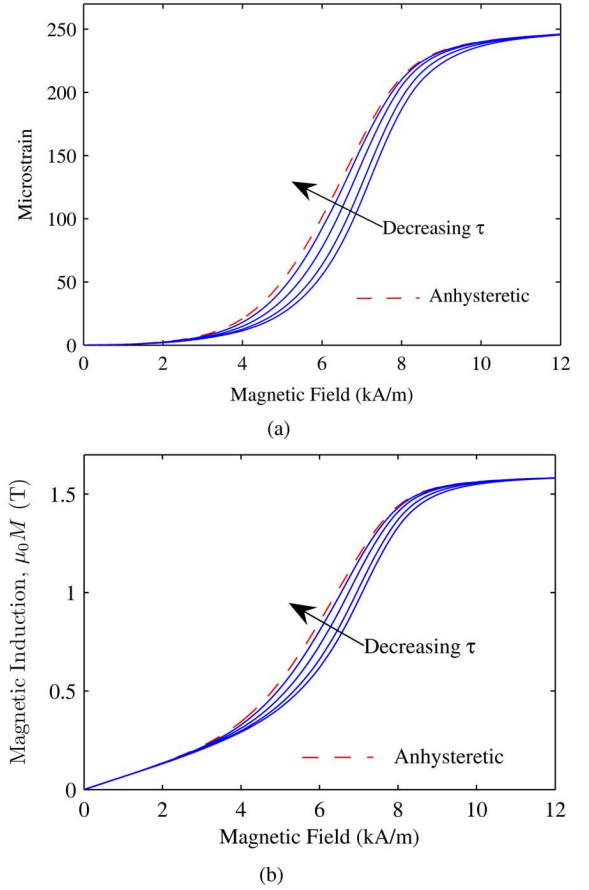


Fig. 8. (a) Magnetostriction model and (b) magnetization model for decreasing time constant  $\tau$  including the anhysteretic steady-state model.

$$S = \frac{\int_{-1}^1 \frac{3}{2} \lambda_{001} \bar{M}_r^2 e^{-G(\bar{M}_r, T, H)V/k\theta} d\bar{M}_r}{\int_{-1}^1 e^{-G(\bar{M}_r, T, H)V/k\theta} d\bar{M}_r}. \quad (22)$$

### III. COMPARISON WITH EXPERIMENTAL DATA

The model is compared to major loop measurements of both unannealed and annealed  $\text{Fe}_{81.6}\text{Ga}_{18.4}$ . The samples are research-grade highly textured polycrystals from Etrema Products Inc., which have a large fraction of the crystallites with the [001] direction oriented within five degrees of the rod axis. Galfenol manufactured in this fashion exhibits cubic anisotropy when unannealed and tetragonal anisotropy when annealed [2]. The measurements were performed in a closed magnetic circuit with ramp current inputs to a solenoid that take 40 seconds to go from positive saturation to negative saturation. Because of the nonlinear nature of the magnetic circuit, the applied magnetic field was not a perfect ramp. However, perfect ramp inputs were used in the model. Because the tests were quasi-static, the shape of the major loop is not affected by the shape of the input field provided it is monotonic as it increases to positive saturation and monotonic as it decreases to negative saturation.

To evaluate the accuracy of the model and its sensitivity to operating conditions, we optimized the model parameters with a least-squares algorithm for four different cases, each with a different level of compressive stress (Tables II and III) for both unannealed and annealed material. The parameters  $\mu_0 M_s$  and

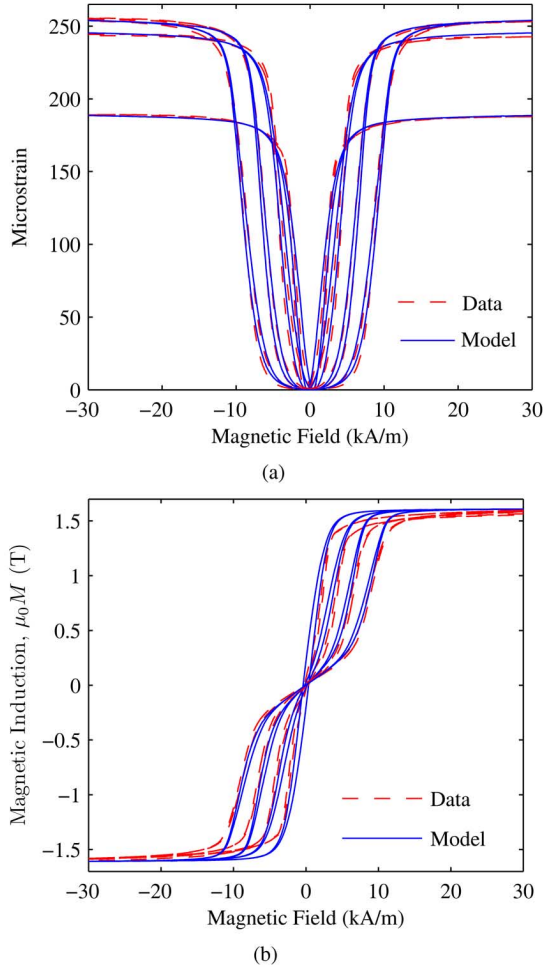


Fig. 9. Comparison of model with experimental data of unannealed  $\text{Fe}_{81.6}\text{Ga}_{18.4}$  with stresses of  $-1.38$ ,  $-13.9$ ,  $-27.6$ , and  $-41.4$  MPa. Each model curve was generated with parameters obtained through minimization of the error with the respective curve.

$3/2\lambda_{001}$  were measured directly as  $1.62$  T and  $260$   $\mu\text{strain}$ , respectively. Initial values for the anisotropy constants were estimated from the  $M$ - $H$  curve as described in Section II-C. For the magnetostriction measurements, the zero-field magnetostriction is defined as zero for each curve. Zero magnetostriction for model equation (20) is the  $90^\circ$  moment orientation that is only achieved at high stress levels. Hence, to compare the model to measurements, the zero-field magnetostriction must be subtracted from the model.

The objective function of the optimization algorithm was the sum of the square of the errors in the magnetostriction at each data point. The magnetostriction was used partly because of the difference in the magnetostriction and magnetization-squared behavior shown in Fig. 7 and because the magnetostriction is of greater interest for transducer design. If the magnetostriction were due solely to domain rotation and domain rotation were the only magnetization process, the magnetostriction versus field and magnetization-squared versus field would be nearly identical when plotted as a relative magnitude. Since they are not, there are unmodeled effects present such as domain wall motion and material defects.

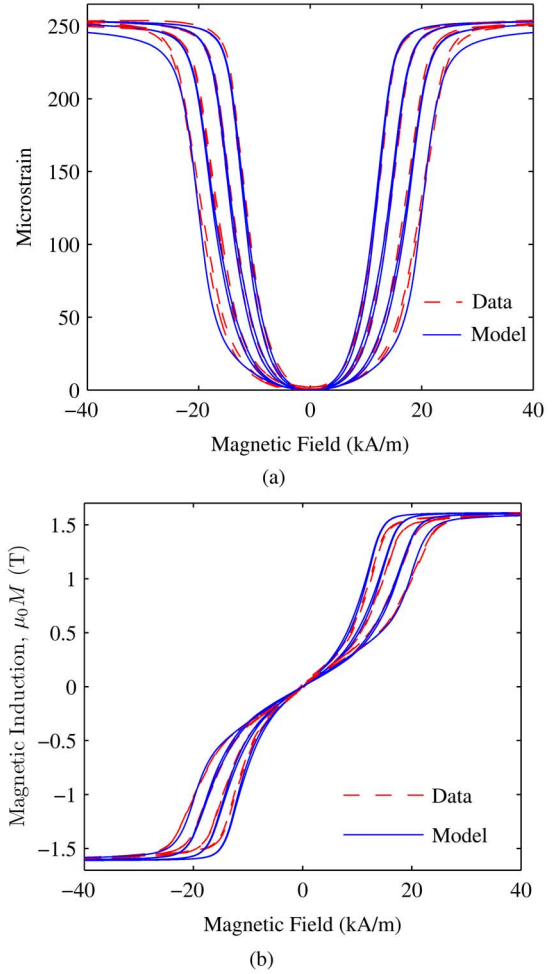


Fig. 10. Comparison of model with experimental data of annealed  $\text{Fe}_{81.6}\text{Ga}_{18.4}$  with stresses of  $-1.38$ ,  $-13.9$ ,  $-27.6$ , and  $-41.4$  MPa. Each model curve was generated with parameters obtained through minimization of the error with the respective curve.

Because of our choice of objective function, the error in the magnetostriction, Fig. 10(a), is smaller than the error in the magnetization, Fig. 10(b). Tables II and III show the parameters optimized for each stress case and some amount of variability in the parameters is noted. While clear trends in the parameters with respect to stress are not evident, the errors are larger for the unannealed, low-stress cases 1 and 2. This may be attributed to domain wall motion being a more significant magnetization process when stress is low in unannealed material. Both stress and annealing tend to align magnetic moments perpendicular to the rod; rotation then becomes the dominant process as moments rotate into the direction along the rod in response to an applied field.

The model accurately quantifies both the shape and the small amount of hysteresis present in the data. Fig. 9(a) shows that the thermal energy formulation in Section II-D describes the ability of a compressive stress to encourage  $90^\circ$  initial moment orientations. The model also describes the decrease in hysteresis to near nonexistence due to annealing and applied stress (Fig. 10). For the fourth stress level ( $-41.4$  MPa), the uniaxial anisotropy and stress were high enough to require use of the constitutive equations for a single-well potential (21) and (22). Fig. 11 shows

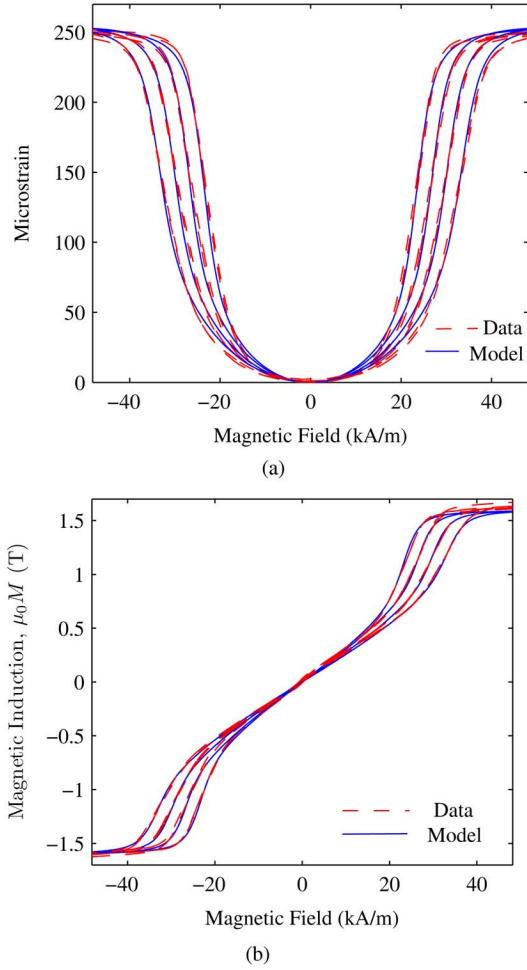


Fig. 11. Comparison of the single-well model with experimental data of annealed  $\text{Fe}_{81.6}\text{Ga}_{18.4}$  for stresses of  $-55.2$ ,  $-69$ ,  $-82.7$ , and  $-96.5$  MPa. Each model curve was generated with parameters obtained through minimization of the error with the respective curve.

measurements of the annealed material at higher stresses and further illustrates the accuracy of the single-well constitutive model.

The model parameters are related to physical properties of the data. The saturation intrinsic flux density  $\mu_0 M_s$  and magnetostriction (when sufficient prestress is applied) achieved at high magnetic field. The effect of the anisotropy constants  $K_2$  and  $K_4$  is manifested through relations (11) and (12), which describe how the low-field slope and the start of the burst region change with stress. This change can be seen in the data [see Figs. 9(b), 10(b), and 11(b)] where the low-field slope decreases and the start of the burst region is delayed with increasing stress. The effect of the thermal energy  $k_B \theta / V$  is evident in the smooth transitions of the burst region as opposed to sharp jumps as predicted by minimization of the Gibbs energy. Finally, the time constants are related to the amount of hysteresis in the data where less hysteresis implies a smaller time constant.

Fig. 12 illustrates the performance of the model when the same parameter set is used on the four stress cases; the parameters were optimized for the first and third stress values with the error in the magnetostriction used as the optimization

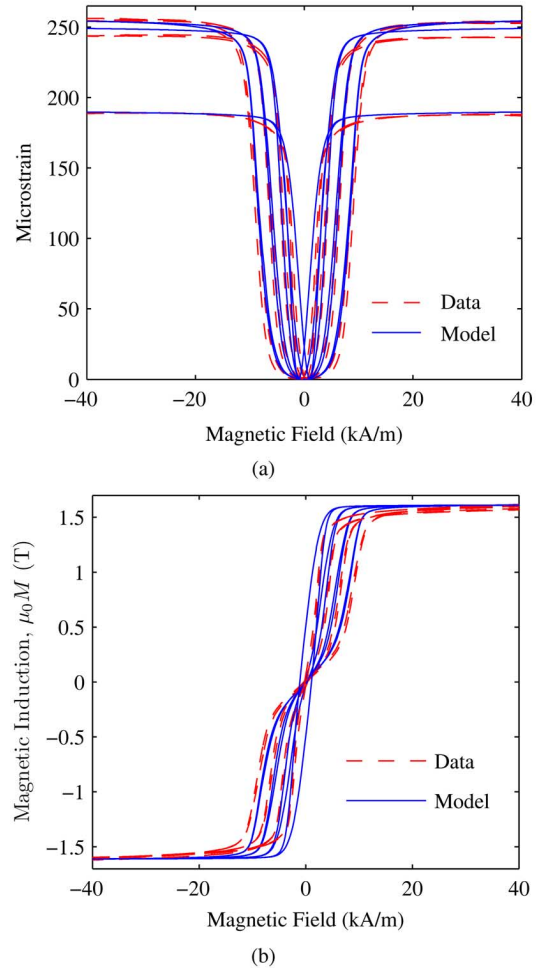


Fig. 12. Comparison of model with experimental data of unannealed  $\text{Fe}_{81.6}\text{Ga}_{18.4}$  with stresses of  $-1.38$ ,  $-13.9$ ,  $-27.6$ , and  $-41.4$  MPa. Each model curve was generated with the same set of parameters.

objective function. The maximum percent error was 3.6%, 5.6%, 1.3%, and 1.3% for stress cases 1–4, respectively (compare to Table II). The error is again larger in cases 1 and 2 where the stress is not large enough to achieve complete alignment of moments perpendicular to the rod axis.

#### IV. CONCLUDING REMARKS

A linear, time-variant, state-space constitutive model is presented that quantifies the nonlinear magnetization and magnetostriction of Galfenol alloys. The effects of external magnetic fields, stresses, and stress annealing on the magnetization and magnetostriction of Galfenol are modeled by quantifying the coupling between magnetocrystalline anisotropy, magnetoelastic, Zeeman, and thermal energies. A triple-valued magnetization kernel characterized by a triple-well Gibbs energy potential provides an understanding of both the low permeability and burst regions of the major loop magnetization curve. Boltzmann statistics is used to describe the distribution and rotations of magnetic moments. This provides a physical basis for understanding the key features of the magnetization and magnetostriction loops as well as the ability of a compressive stress to align magnetic moments  $90^\circ$  from the  $z$ -axis for maximum magnetostriction. A small amount of hysteresis is

naturally present in the model due to anisotropy and agrees well with experimental measurements. Unaccounted-for effects such as pinning sites are likely to contribute to the magnetic hysteresis as well.

#### ACKNOWLEDGMENT

The authors thank J. Restorff (Naval Surface Warfare Center, Carderock Division) for providing the experimental data used for model validation. This work was supported by the Office of Naval Research under Grant N000140610530.

#### REFERENCES

- [1] P. R. Downey and A. B. Flatau, "Magnetoelastic bending of Galfenol for sensor applications," *J. Appl. Phys.*, vol. 97, pp. 10R505–10R505-3, 2005.
- [2] J. B. Restorff, M. Wun-Fogle, A. E. Clark, and K. B. Hathaway, "Induced magnetic anisotropy in stress-annealed Galfenol alloys," *IEEE Trans. Magn.*, vol. 42, no. 10, pp. 3087–3089, Oct. 2006.
- [3] J. Atulasimha and A. B. Flatau, W. D. Armstrong, Ed., "Energy-based model for the magnetostrictive behavior of polycrystalline iron-gallium alloys," in *Smart Structures Mater. 2006: Active Materials: Behavior Mechanics*, ser. Proc. SPIE, 2006, vol. 6170, pp. 617000M-1–617000M-9.
- [4] W. D. Armstrong, "Magnetization and magnetostriction processes," *J. Appl. Phys.*, vol. 81, no. 5, pp. 23 217–2326, 1997.
- [5] D. Aeyels, R. Sepulchre, and J. Peuteman, "Asymptotic stability conditions for time-variant systems and observability: Uniform and non-uniform criteria," *Math Control Signals Syst.*, vol. 11, 1998.
- [6] E. Du Trémolet de Lacheisserie, *Magnetostriction*. Boca Raton, FL: CRC, 1993.
- [7] S. Rafique, J. R. Cullen, M. Wuttig, and J. Cui, "Magnetic anisotropy of FeGa alloys," *Appl. Phys.*, vol. 95, no. 11, pp. 6939–6941, 2004.
- [8] C. Kittel, "Physical theory of ferromagnetic domains," *Rev. Mod. Phys.*, vol. 21, no. 4, pp. 541–583, Oct. 1949.
- [9] C. Appino, M. Valsania, and V. Basso, "A vector hysteresis model including domain wall motion and coherent rotation," *Physica B*, vol. 275, no. 1–3, pp. 103–106, 2000.
- [10] L. Néel, *Ann Geophysicae*, vol. 5, p. 99, 1949.
- [11] R. C. Smith, M. J. Dapino, T. R. Braun, and A. P. Mortensen, "A homogenized energy framework for ferromagnetic hysteresis," *IEEE Trans. Magn.*, vol. 42, no. 4, pp. 1747–1769, Apr. 2005.
- [12] B. D. Cullity, *Introduction to Magnetic Materials*. Reading, MA: Addison-Wesley, 1972.
- [13] R. C. Smith, *Smart Material Systems: Model Development*, ser. Frontiers in Applied Mathematics. Philadelphia, PA: SIAM, 2005.
- [14] R. C. Smith, S. Seelecke, Z. Ounaies, and J. Smith, "A free energy model for hysteresis in ferroelectric materials," *J. Intell. Mater. Syst. Struct.*, vol. 14, no. 11, pp. 719–739, Nov. 1, 2003.
- [15] S. Seelecke and I. Muller, "Shape memory alloy actuators in smart structures: Modeling and simulation," *Appl. Mech. Rev.*, vol. 57, no. 1, 2004.
- [16] D. C. Jiles, *Introduction to Magnetism and Magnetic Materials*. London, U.K.: Chapman & Hall, 1995.
- [17] R. A. Kellogg, A. Flatau, A. E. Clark, M. Wun-Fogle, and T. Lograsso, "Quasi-static transduction characterization of Galfenol," *J. Intell. Mater. Syst. Struct.*, vol. 16, pp. 471–479, 2005.

Manuscript received November 17, 2007; revised March 19, 2008. Corresponding author: M. J. Dapino (e-mail: dapino.1@osu.edu).